Prospects for the detection rate of very-high-energy γ-ray emissions from short γ-ray bursts with the HADAR experiment*

Qi-Ling Chen (陈琪凌)[1] Pei-Jin Hu (胡珮瑾)[1] Jing-Jing Su (苏菁菁)[1] Ming-Ming Kang (康明铭)[1†]
Yi-Qing Guo (郭义庆)[2,3‡] Tian-Lu Chen (陈天禄)[4§] Dan-Zeng Luo-Bu (单增罗布)[4] Yu-fan Fan (范雨凡)[4]
You-Liang Feng (冯有亮)[4] Qi Gao (高启)[4] Quan-Bu Gou (苟全补)[2] Hong-Bo Hu (胡红波)[2,3]
Hai-Jin Li (厉海金)[4] Cheng Liu (刘成)[2] Mao-Yuan Liu (刘茂元)[4] Wei Liu (刘伟)[2]
Xiang-Li Qian (钱详利)[5,4] Bing-Qiang Qiao (乔冰强)[2] Hui-Ying Sun (孙慧英)[5] Xu Wang (王旭)[5]
Zhen Wang (王振)[6] Guang-Guang Xin (辛广广)[7] Yu-Hua Yao (姚玉华)[8] Qiang Yuan (袁强)[9]
Yi Zhang (张毅)[9] Bing Zhao (赵兵)[2]

[1]College of Physics, Sichuan University, Chengdu 610064, China
[2]Key Laboratory of Particle Astrophysics, Institute of High Energy Physics, Chinese Academy of Sciences, Beijing 100049, China
[3]University of Chinese Academy of Sciences, 19 A Yuquan Rd, Shijingshan District, Beijing 100049, China
[4]The Key Laboratory of Cosmic Rays (Tibet University), Ministry of Education, Lhasa 850000, China
[5]School of Intelligent Engineering, Shandong Management University, Jinan 250357, China
[6]Tsung-Dao Lee Institute, Shanghai Jiao Tong University, Shanghai 200240, China
[7]School of Physics and Technology, Wuhan University, Wuhan 430072, China
[8]College of Physics, Chongqing University, Chongqing 401331, China
[9]Key Laboratory of Dark Matter and Space Astronomy, Purple Mountain Observatory, Chinese Academy of Sciences, Nanjing 210008, China

Abstract: The observation of short gamma ray bursts (SGRBs) in the TeV energy range plays an important role in understanding the radiation mechanism and probing potential new physics, such as Lorentz invariance violation (LIV). However, no SGRBs have been observed in this energy range owing to the short duration of SGRBs and the weakness of current experiments. New experiments with new technology are required to detect the very high energy (VHE) emission of SGRBs. In this study, we simulate the VHE γ-ray emissions from SGRBs and calculate the annual detection rate with the High Altitude Detection of Astronomical Radiation (HADAR) experiment. First, a set of pseudo-SGRB samples is generated and checked using the observations of the Fermi-GBM, Fermi-LAT, and Swift-BAT measurements. The annual detection rate is calculated from these SGRB samples based on the performance of the HADAR instrument. As a result, the HADAR experiment can detect 0.5 SGRBs per year if the spectral break-off of γ-rays caused by the internal absorption and Klein-Nishina (KN) effect is larger than 100 GeV. For a GRB090510-like GRB in HADAR's view, it should be possible to detect approximately 2000 photons considering the internal absorption and KN effect. With a time delay assumption due to LIV effects, a simulated light curve of GRB090510 has evident energy dependence. We hope that the HADAR experiment can perform SGRB observations and test our calculations in the future.

Keywords: HADAR, simulation, gamma ray burst, cosmic ray

DOI: 10.1088/1674-1137/ace3ac

I. INTRODUCTION

Gamma ray bursts (GRBs) are some of the most powerful explosions in the universe and can last from 10 ms to several hours as prompt emissions, releasing most of their energy in the form of photons from 30 keV to a few MeV. The properties of GRBs mainly include two components of temporal and spectral information. First, from the perspective of the temporal property, its prompt phase has a bimodal duration distribution separated at $t \sim 2$ s, indicating that there are two different groups, that is, long GRBs (LGRBs) with $t_{\rm LGRB} > 2\ s$ and short GRBs (SGRBs) with $t_{\rm SGRB} < 2\ s$ [1, 2]. LGRBs are likely formed by the collapse of massive star cores [3, 4],

Received 3 April 2023; Accepted 5 July 2023; Published online 6 July 2023
* Supported by the National Natural Science Foundation of China (12263004, 12263005, 12275279).
† E-mail: kangmm@scu.edu.cn
‡ E-mail: guoyq@ihep.ac.cn
§ E-mail: chentl@ihep.ac.cn

whereas SGRBs are thought to originate from the coalescence of compact binary systems, such as binary neutron stars (BNSs) and neutron star-black hole (NS-BH) systems [5−7]. The associated events GW170817/GRB170817A [8] from a BNS merger make the assumption grounded that BNS mergers are sources (or parts of the sources) of SGRBs. For spectral properties, a two-component structure has been revealed above tens of MeV. At low energy, an experiential Band-function can describe observations well [9, 10], which is possibly induced by the synchrotron radiation process [11−14]. At high energy, the model predicts that another component generated from the inverse-Compton (IC) process should exist [15−18]. In the past few decades, great achievements have been made in experimental measurements studying temporal and spectral characteristics. It is evident that the measurements are relatively rich at low energy, but observations in the TeV band are more desirable.

A milestone was reached in the observation of γ-ray emissions in the TeV band in recent years. The Major Atmospheric Gamma Imaging Cherenkov (MAGIC) and High Energy Stereoscopic System (H.E.S.S.) experiments discovered very high energy (VHE) γ-ray emissions in GRB190114C and GRB180720B [19, 20]. Following these observations, the H.E.S.S. experiments detected photons with energies of up to 4 TeV from GRB190829A, during 4 hr to 56 hr after the trigger time [21]. Moreover, the brightest GRB221009A was recently observed in a multi-band. It is exciting that the most energetic photons can reach 18 TeV [22], as detected by the Large High Altitude Air Shower Observatory (LHAASO). This new discovery opened the observation window of the γ-ray emissions of GRBs in the TeV band and confirmed the new radiation mechanism expected by the model, known as the IC process [15−18]. These discoveries shined a new light on the central engine and radiation mechanism and probed potential new physics, such as Lorentz invariance violation (LIV) and dark matter (DM) [23−25]. It is unfortunate that the γ-ray emissions at TeV energies have only been observed at the afterglow phase of LGRBs. No prompt emission has yet been observed for GRBs at this energy band, let alone SGRBs. Despite this, TeV γ-ray emissions from SGRBs can play very important roles in exploring LIV, which is the hypothesis of several theories of quantum gravity, benefiting from the short duration of SGRBs. Therefore, scientists are highly anticipating γ-ray observation results in the TeV energy region.

Space-borne and ground-based experiments have both contributed to setting limits on LIV. GRB090510 is a typical bright SGRB among high-energy observations, with a photon observed at 31 GeV arriving 0.829 s after the trigger of the Fermi-GBM. This SGRB provides conditions to constrain the LIV effect and provides a lower limit for the linear modification of the photon dispersion relationship, that is, $E_{\rm QG,1} > 1.49\times10^{19}$ GeV [26], which is the best lower limit. However, only one photon was detected above 10 GeV by the Fermi-LAT in this work [26], and an event number with high statistics is better for confirmation of this important result. The shortage of space-borne experiments includes a limited effective area of ~1 m^2, which leads to insufficient sensitivity in the high-energy range. Imaging atmospheric Cherenkov telescope (IACT) experiments have high sensitivity above an energy of 100 GeV; however, the fatal weakness is their field of view (FOV), with a value of only several degrees [27−29]. However, the Cherenkov Telescope Array (CTA) will detect prompt emissions from SGRBs when they are slewed to the source before BNS mergers [30]. The traditional arrays of CR detectors, such as the High-Altitude Water Cherenkov (HAWC) and LHAASO, have good performance above TeV energy and a wide FOV, but these arrays cannot be compared with IACT detectors in the 100 GeV energy range. The optimal choice is an IACT with a wide FOV, such as the High Altitude Detection of Astronomical Radiation (HADAR) project. Therefore, it is necessary to know the detection capability of SGRBs for the HADAR experiment. In this study, the annual detection rate based on a set of pseudo-SGRB samples is generated and checked with the observations of space-borne experiments.

This paper is organized as follows: First, we provide a brief introduction to the HADAR experiment and its performance parameters in Section II. Then, to predict the detection rate of SGRBs with HADAR as reliably as possible, we model the pseudo-SGRBs and the detecting process considering the performance of the detectors of both the Fermi-GBM (for a consistency check) and HADAR. The simulation methods and results are presented in Sections III and IV, respectively. In Section IV, we also describe the simulation of the observational results of GRB090510 in HADAR's case, given as a light curve considering LIV effects. In Section V, we describe the conclusion of our findings.

II. HADAR EXPERIMENT

The HADAR project is proposed for construction in YangBaJing, Tibet of China, at an altitude of 4300 m. As shown in Fig. 1, this project has a hybrid array, which includes the two parts: water lenses and traditional scintillators.

The water lens array is composed of four of the same telescopes. The diameter of each lens is 5 m, the distance between two lenses is 100 m, and the four lenses form a square. The right panel of Fig. 1 presents the detailed profile structure of a single water lens, which mainly consists of an acrylic spherical cap lens with a diameter of 5 m, a cylindrical tank with a radius of 4 m and a height of

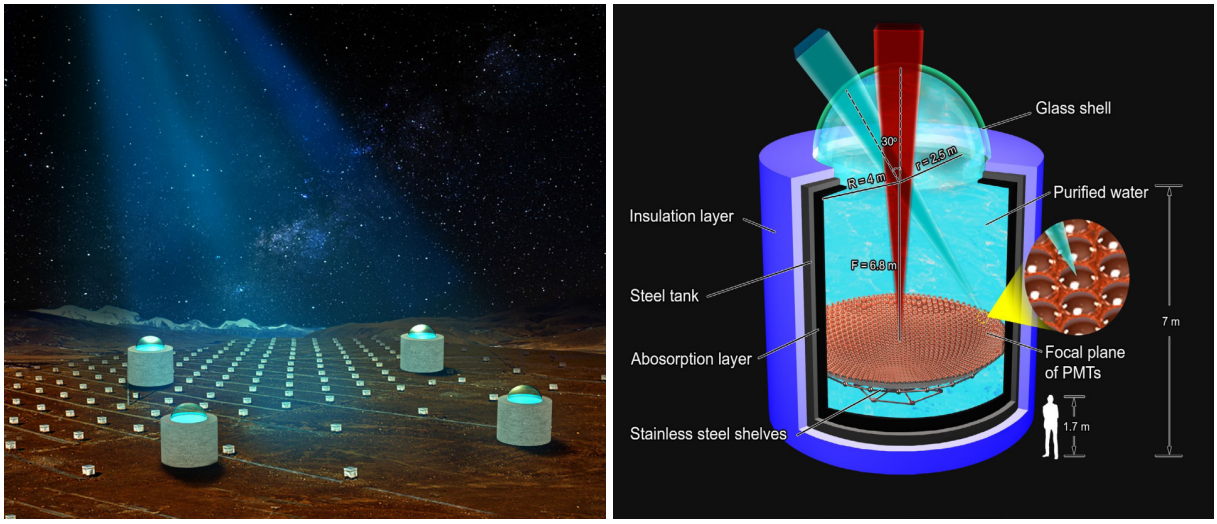

Fig. 1. (color online) HADAR project [31]. Left: Layout of the HADAR array with water lenses. Right: Profile design of each telescope.

7 m, and a camera with an array of 18, 961 photomultiplier tubes (PMTs), each 5 cm in diameter. A steel tank, which contains an absorption layer in the inside wall and a thermal insulation material coating on the outer wall, is filled with purified water to concentrate radiation emissions to the PMTs. The PMTs are placed in the focal plane of the lens and arranged as a series of concentric ring matrixes supported by a stainless-steel space frame. The water lens array is designed to focus on transient sources, such as GRBs and active galactic nuclei (AGNs), in the northern sky to measure primary γ-rays in the energy range from 10 GeV to 100 TeV. Owing to the properties of the water lens, it has an FOV of 0.84 sr (30° field angle), which is almost one order of magnitude larger than that of IACTs such as H.E.S.S., MAGIC, and CTA [27–29]. It is more important that the effective area, angular resolution, and energy resolution at the 300 GeV energy can reach 10000 m^2, 0.5^0, and 20%, respectively, which is comparable to those of H.E.S.S. and MAGIC, except for the angular resolution. The water lens detection design can meet the observation requirements of our physical targets.

The scintillator array is composed of 100 detectors and is designed to perform joint observations with a water lens. The installation and maintenance of a scintillator detector are simple, and such detectors can achieve long-term stable performance and good time resolution and are widely used in extensive air shower (EAS) arrays [32]. The frame structure is composed of stainless steel with an upside-down pyramidal shape, known as a box of light guide (BLG). The interfaces of a BLG are light-tight, with a reflective material, DuPont Tyvek, covering the inner surface with the purpose of significantly increasing the efficiency of light collection. A KD2000 plastic scintillator is adopted with dimensions of 1 m × 1 m × 2 cm and placed on top of the frame. A PMT with a diameter of two inches is chosen and installed at the bottom. When charged particles induced by the primary CRs pass through the scintillator, photons are generated. Some of these photons can be refracted several times in the BLG, and some finally reach and are collected by the PMT. The main function of the scintillator detector is to measure the coincidence with the water lens and confirm the performance of the water lens.

Following the methods of H.E.S.S. and CTA [33, 34], we can obtain the performance of HADAR, which includes the effective area, angular resolution, and point spread function (PSF). The effective area and angular resolution are shown in Ref. [35]. r_{80} is the radius of the circle around the center of gravity of the image, containing 80% of the total intensity. In simulation, r_{80} for HADAR is 15 mm, and the focal length is 680 cm. Therefore, the PSF is 0.13 degrees.

III. MODELING SGRB SAMPLES

To estimate the detection rate of the prompt emissions from SGRBs for HADAR, we adopt a simulation method based on Monte Carlo. A set of SGRB samples is generated according to the phenomenological models of their intrinsic parameters, such as space density, luminosity, energy spectra, temporal duration, and extragalactic background light (EBL) attenuation. The expected detection rate is calculated using the spectra for each GRB and the HADAR sensitivity.

A. Redshift distribution

SGRBs are simulated with an isotropic distribution on the sky. The redshift distribution is used to generate the distance of the SGRBs. The redshift distribution de-

scribes the number of SGRBs per unit redshift bin $\mathrm{d}z$ per unit (observed) time $\mathrm{d}t$, which is expressed as [36]

$$\frac{\mathrm{d}N}{\mathrm{d}t\mathrm{d}z} = \frac{\dot{\rho}(z)}{1+z}\frac{\mathrm{d}V(z)}{\mathrm{d}z}, \tag{1}$$

where

$$\frac{\mathrm{d}V(z)}{\mathrm{d}z} = \frac{c}{H_0}\frac{4\pi D_L^2}{(1+z)^2[\Omega_m(1+z)^3+\Omega_\Lambda]^{1/2}}. \tag{2}$$

In this study, we adopt $H_0 = 67.4\ \mathrm{km\ s^{-1}\ Mpc}$, $\Omega_m = 0.315$, and $\Omega_\Lambda = 0.685$ [37]. In addition, $\dot{\rho}(z)$ is the event rate density at z (in units of $\mathrm{Gpc^{-3}\ yr^{-1}}$), which is [38, 39]

$$\dot{\rho}(z) \propto (1+z)\int_{t_{\min}}^{t_{\max}} R_F[z_f(t_d,z)]P(t_d)\mathrm{d}t_d, \tag{3}$$

where $P(t_d) \propto 1/t_d$, $t_{\min} = 20\ \mathrm{Myr}$ is the minimum delay time for a BNS system to evolve to merge, $t_{\max}$ is the age of the universe at the time of merging $t(z)$, and $R_F[z_f(t_d,z)]$ is the star formation history (SFH), which is adopted from Ref. [40]. The relationship between z, z_f, and t_d is described in Eq. (4) below. We normalize the event rate density $\dot{\rho}(z)$ with $1540^{+3200}_{-1220}\ \mathrm{Gpc^{-3}\ yr^{-1}}$ [8], which corresponds to the local event rate density at $z = 0$.

The delay time t_d between the formation of the binary system $t_f(z_f)$ and the age of the universe at the time of the merger $t(z)$ is given as

$$t_d = \int_z^{z_f} \frac{\mathrm{d}z'}{H_0(1+z')[\Omega_m(1+z)^3+\Omega_\Lambda]^{1/2}}, \tag{4}$$

where z_f and z represent the redshifts at which the BNS systems form and merge, respectively.

B. Luminosity function

The luminosity of SGRBs can be parameterized as a broken power law, as widely adopted in other studies:

$$\Phi(L) = A\begin{cases}\left(\frac{L}{L_c}\right)^{\alpha}, & L \le L_c\\ \left(\frac{L}{L_c}\right)^{\beta}, & L > L_c\end{cases} \tag{5}$$

where A is the normalization constant, L_c is the break luminosity, and α and β are the power-law indices. Here, we adopt $\alpha = -1.95$, $\beta = -3$, $L_c = 2\times10^{52}\mathrm{erg\ s^{-1}}$, $L_{\min} = 1\times10^{49}\ \mathrm{erg\ s^{-1}}$ [41]. The luminosity function is used to generate the peak luminosity L_p.

C. Prompt emission spectrum

The prompt emission spectrum of GRBs may include two spectral components: a non-thermal Band component (Band) and a non-thermal power law component extending to high energies (Extra). In this study, we assume all of the pseudo-SGRBs have a Band + Extra spectrum.

The Band function is usually used to fit the spectrum of a GRB when the detector's energy band is sufficiently wide. The Band function is [9, 10]

$$N_{\mathrm{Band}}(E) = A_0\begin{cases}\left(\frac{E}{E_0}\right)^{\alpha}\exp\left(-E/E_p\right), & E \le E_c\\ \left(\frac{E_c}{E_0}\right)^{\alpha-\beta}\exp(\beta-\alpha)\left(\frac{E}{E_0}\right)^{\beta}, & E > E_c\end{cases} \tag{6}$$

where $E_0 = 100\ \mathrm{keV}$, $E_c = (\alpha-\beta)E_p$, A_0 is the normalization constant in units of photons $\mathrm{s^{-1}\ cm^{-2}\ keV^{-1}}$, which is detetermined by the average luminosity $L_{\mathrm{ave}} = 0.31L_p$ [42], α and β are the low and high energy photon indices, respectively, and E_p is the peak energy of the spectrum. In this study, α and β are adopted from the observations of the Fermi-GBM [43], and E_p is determined by the $E_p - L_p$ relationships examined in Ref. [44].

Beyond the Band function, a high-energy and power law spectral component is necessary to fit the spectrum in certain GRBs [26, 45, 46]. The power law component is the dominant contribution to the high-energy prompt emission beyond tens of GeV. Here, we introduce the extra component for GRB spectra.

$$N_{\mathrm{ext}} = B_0\left(\frac{E}{E_0}\right)^{\beta_{\mathrm{ext}}}, \tag{7}$$

B_0 is the normalization constant, similar to A_0, which is determined by the luminosity of the extra power law spectrum L_{ext}. The luminosity ratio $R_{\mathrm{ext}} = L_{\mathrm{ext}}/L_{\mathrm{ave}}$ and photon index β_{ext} are used to describe the extra component. L_{ave} is the luminosity of the Band component. We take $R_{\mathrm{ext}} = 0.1$ and $\beta_{\mathrm{ext}} = 1.75$ by default. Therefore, in our study, the spectrum of SGRBs is expressed as

$$N(E) = N_{\mathrm{Band}}(E) + N_{\mathrm{ext}}(E), \tag{8}$$

Photons with high energies may be strongly attenuated because of internal absorption, the Klein-Nishina (KN) effect [47–49], and EBL absorption.

Following [31], an exponential cutoff on the spectrum is used to describe the internal absorption and KN effect:

$$N_{\mathrm{cut}}(E) = N(E)\exp(-E/E_{\mathrm{cut}}), \tag{9}$$

here, E_{cut} is the cutoff energy. The cases of 30 GeV, 50

GeV, 100 GeV, 1 TeV and no energy cutoff are considered.

High-energy photons from distant astrophysical sources are subject to attenuation because of two-photon pair production with EBL. The spectrum with EBL attenuation is expressed as

$$N_{\rm EBL}(E) = N(E)\exp(-\tau(E,z)), \tag{10}$$

where $\tau(E,z)$ is the optical depth for the γ-rays at energy E. The EBL attenuation introduced in Ref. [35] is used by default.

The spectrum considering EBL and the exponential cutoff is expressed as

$$N_{\rm EBL+cut}(E) = N(E)\exp[-(\tau(E,z)+E/E_{\rm cut})]. \tag{11}$$

Figure 2 shows the energy spectrum of the SGRBs, where EBL and the exponential cutoff are considered.

D. Duration of prompt emission

The duration of the GRBs is approximately estimated using T_{90}, which corresponds to the time in which 90% of the counts arrive. T_{90} is described as [42, 50]

$$T_{90} = (1+z)\frac{E_{\rm iso}}{L_{\rm ave}}, \tag{12}$$

where the isotropic energy $E_{\rm iso}$ is calculated using [44]

$$E_{\rm iso} = 10^{51.42\pm0.15}{\rm erg}\left(\frac{E_p}{774.5\ {\rm keV}}\right)^{1.58\pm0.28}. \tag{13}$$

The average luminosity $L_{\rm ave}$ is calculated using $L_{\rm ave} = 0.31L_p$.

E. Significance

Based on the preparations above, a group of GRBs can be constructed using Monte Carlo with the definite parameters $(\alpha,\beta,E_p,L_p,T_{90},z)$. Then, the sample is ready for a quality check with Fermi-GBM observations. The significance for every GRB is calculated based on the expected signal and background number, that is, $N_{\rm signal}$ and $N_{\rm bkg}$, respectively. The signal can be obtained as

$$N_{\rm signal} = \int_{E_{\rm min}}^{E_{\rm max}} N_{\rm EBL}(E)T_{90}A_{\rm eff}^{\gamma}(E,\theta){\rm d}E, \tag{14}$$

where T_{90} is described in Eq. (12), and $N_{\rm EBL}(E)$ is the spectrum of the SGRB with EBL. If the exponential cutoff is considered, it will be replaced by $N_{\rm EBL+cut}(E)$. $A_{\rm eff}$ is the effective area of the detector. For HADAR, the

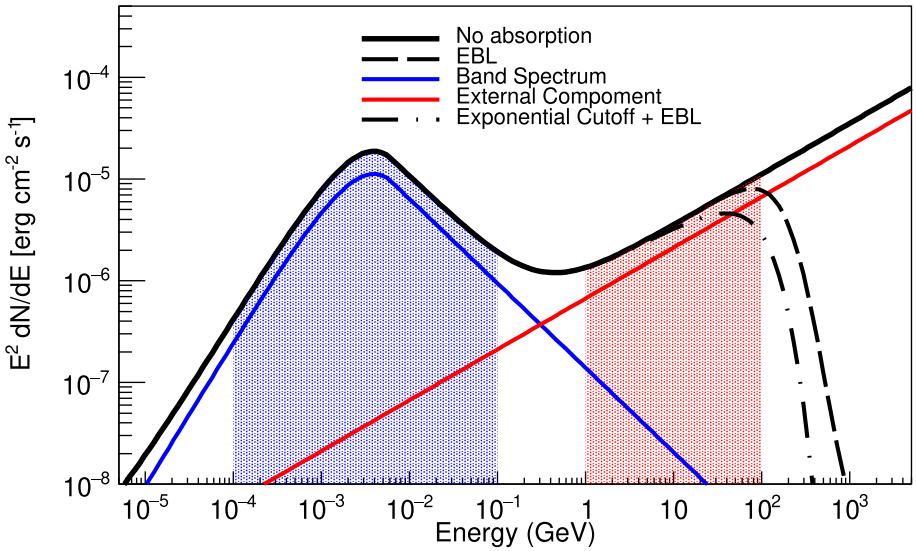

Fig. 2. (color online) Energy spectrum of the Band function considering EBL and the exponential cutoff. The blue and red solid lines represent the spectra of the Band function and extra component, respectively. The dashed line represents the spectrum when considering the EBL absorption of Ref. [35]. The dotted line represents the spectrum considering the exponential cutoff and EBL. These are described in Eqs. (10) and (11). A redshift of $z = 0.903$ is adopted, and the cutoff energy is 100 GeV. The black lines are the sum of the Band function and extra component, which is described in Eq. (8). The values of $\beta_{\rm ext}$ and $R_{\rm ext}$ are −1.5 and 0.1, respectively. $R_{\rm ext}$ represents the ratio of the fluences in the energy ranges of 100 MeV to 100 GeV and 100 keV to 100 MeV, which are the red- and blue-shaded regions, respectively. To distinguish the individual components of the emission from the total combined flux, both the Band spectrum and extra component are scaled by 0.5.

effective area is adopted from Ref. [31]. The integral limit $(E_{\rm min}, E_{\rm max})$ is the detector's energy band, which is (10 GeV, 10 TeV) for HADAR.

For space-borne detectors such as the GBM, $N_{\rm bkg}$ originates from cosmic γ background rates in the corresponding energy bands. For IACT, $N_{\rm bkg}$ results from the cascades of cosmic rays [31, 42]:

$$N_{\rm bkg} = \int_{E_{\rm min}}^{E_{\rm max}} S_p(E) T_{90} A_{\rm eff}^p(E,\theta)\Omega(E){\rm d}E, \tag{15}$$

where $S_p(E)$ represents the spectrum of cosmic rays, $A_{\rm eff}^p$ is the effective area of HADAR corresponding to cosmic rays, and $\Omega(E)$ is the solid angle corresponding to the angular resolution of HADAR. These are given in Ref. [31].

A 5σ deviation is required as a trigger, which is calculated as $N_{\rm signal}/\sqrt{N_{\rm bkg}} > 5$.

F. Check by observations

Data from of the Fermi-GBM is used to check our samples, and the detection rates of the Fermi-GBM, Swift-BAT, and Fermi-LAT are used to verify our detection rate. In the observational results of the Fermi-GBM, 395 SGRBs were observed over ten years. To evaluate the difference between our samples and this observation, $\chi^2_{\rm tot}$ is calculated as $\sum\chi_i^2/\sum N_i^{\rm bin}$, where i denotes $\alpha, \beta, E_p, z, T_{90}$, and the fluence, and $N_i^{\rm bin}$ is the corresponding bin number. The total combined $\chi^2_{\rm tot}$ is 0.81.

The $\alpha, \beta, E_p, z, T_{90}$, and fluence distributions of our phenomenological models and real observations are compared, as shown in Fig. 3. From Fig. 3, we find that our model results are roughly consistent with the real observations of the Fermi-GBM given the experimental uncertainties.

Table 1 shows the real detection rates compared with simulated rates of the Fermi-GBM, Swift-BAT, and Fermi-LAT. Figure 4 shows the cumulative simulated detection rates as a function of detected photons. We find that at a low or high energy, our simulated detection rates are roughly consistent with the real detection rates

IV. RESULTS

The results of our study include two parts: the detected event rates of SGRBs, and a pseudo light curve for GRB090510 simulated with the HADAR experiment, which reflects HADAR's capacity to detect VHE SGRBs with sufficient sensitivity and a wide FOV to observe photons extending to the VHE spectral component.

A. Expected detection rates

The left panel of Fig. 5 presents the expected detection rates between z and $z+{\rm d}z$ for the GBM and HADAR compared with the BNS merger rate. The right panel of Fig. 5 shows the cumulative detection rates of SGRBs. Here, the spectrum with only the Band spectrum or Band and extra power low spectrum is considered. If the single Band spectrum is considered, the expected detection rate for HADAR is 0.49 per year. If the spectrum with the extra power law is considered in the simulation ($R_{\rm ext} = 0.1$), the detection rates are 0.82, 1.2, and 1.6 for $\beta_{\rm ext} = -2.0$, -1.75, and -1.5, respectively.

The left panel of Fig. 6 shows the cumulative detection rate with different energy cut-offs considering the exponential cutoff. With the EBL model of Ref. [35], the expected detection rates are 0.20, 0.38, 0.64, and 1.1 for $E_{\rm cut} = 30$ GeV, 50 GeV, 100 GeV, and 1 TeV, respectively. The right panel of Fig. 6 presents the cumulative detection rate for HADAR with different EBL models. It is shown that the different EBL models have little effect on the expected detection rates for HADAR, which are approximately 0.55 or 1.1 per year for the different EBL models adopted from Refs. [35, 54−56] with or without a 100 GeV energy cutoff.

B. Pseudo light curve of GRB090510

Based on our HADAR model and the parameters of GRB090510 extracted from the observational results [45], including the redshift, spectrum, and considering the model of the LIV effects for the GRB from Ref. [26], a pseudo light curve of the HADAR observation is generated, as shown in panels (c) and (d) of Fig. 7, as well as each photon with the observed time and energy.

To present this light curve, we consider the photon energy distribution to follow the spectrum of a 090510-like GRB combined with EBL attenuation. Then, these photons are detected by HADAR with effective areas and a 20% energy resolution. From the observation of GRB090510, there are seven pulses in the light curve. Therefore, we use them to simulate the light curve detected by HADAR. An assumption is made that the photons

Table 1. Annual detection rates of different experiments. The data of the Fermi-GBM, Swift-BAT, Fermi-LAT are taken from Refs. [51−53].

	Fermi-GBM	Swift-BAT	Fermi-LAT > 100 MeV	Fermi-LAT > 1 GeV	Fermi-LAT > 10 GeV
Observation	39.5	9.32	1.4	0.7	0.1
Simulation	38.9 ± 6.24	8.75 ± 2.96	1.55 ± 1.24	0.78 ± 0.88	0.05 ± 0.23

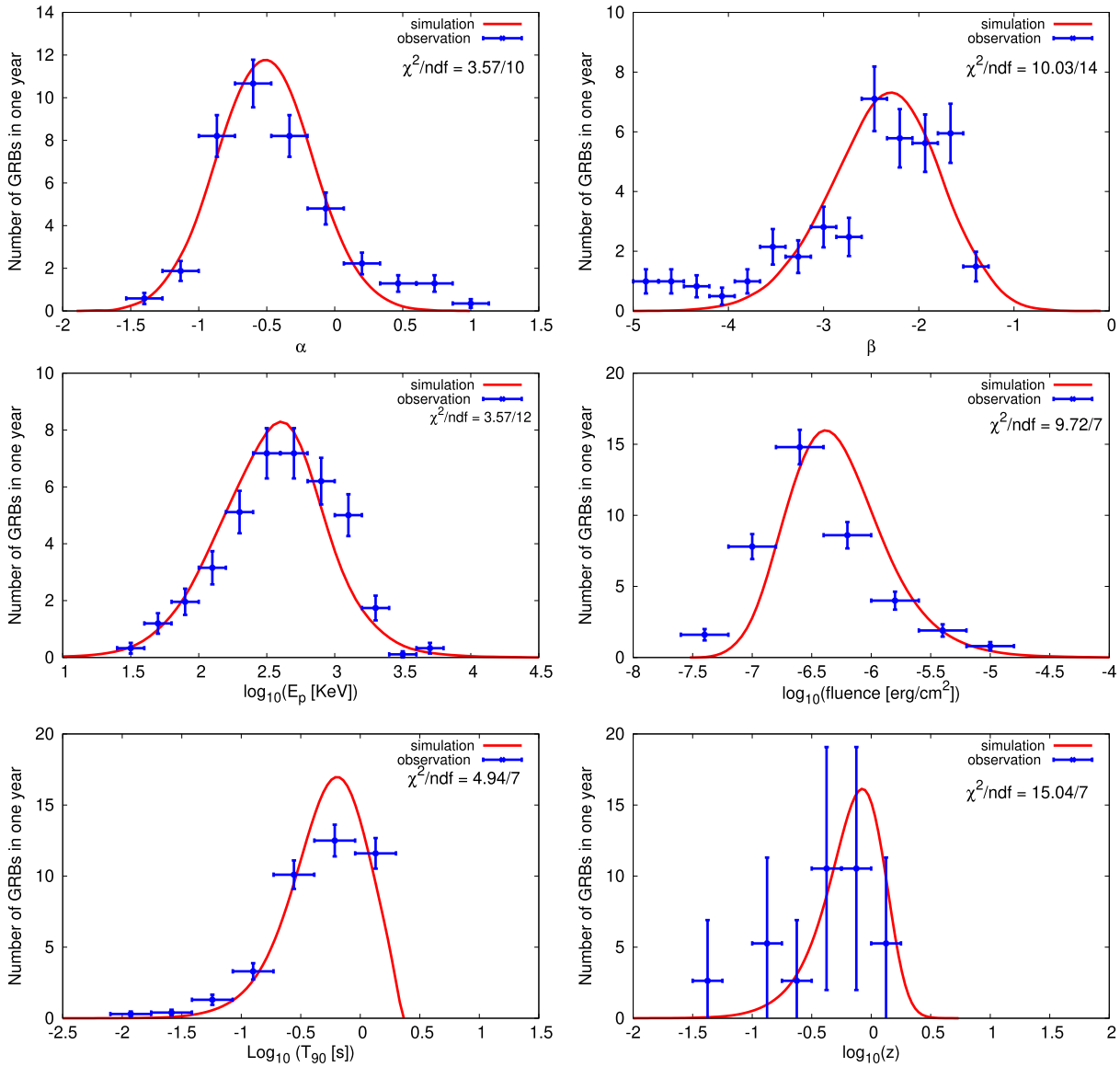

Fig. 3. (color online) Model results of α (top left), β (top right), E_p (middle left), fluence (middle right), T_{90} (bottom left), and redshift z (bottom right). The observation data is taken from the Fermi-GBM.

in a pulse from the source burst at exactly the same time. For the LIV effects, a positive time delay $\Delta t = (\Delta E/E_{\rm QG})D/c$ is included in the simulated arrival time of photons, where $E_{\rm QG} = M_{\rm QG}c^2$ is the Planck energy, D is the co-moving distance from source to detector, and $\Delta E = E_{\gamma,\rm high} - E_{\gamma,\rm low}$. The energy dispersion of the time delay $\Delta t/\Delta E = +0.03$ s/GeV is adopted [26]. From Fig. 7, it is clear that HADAR is better than the Fermi-LAT in the high energy range, which is helpful for providing more constraints on the parameters of LIV effects.

V. CONCLUSIONS

The observations of TeV γ-ray emissions from SGRBs are very important for studying the central engine, radiation mechanism, and potential new physics, such as LIV. Limited by the effective area and narrow FOV of space-borne and ground-based applications with IACT technology experiments, there are still no related results. New experiments are required to have a wide FOV and high sensitivity with IACT technology. The HADAR experiment can fulfill these two requirements simultaneously.

In this study, we produce one SGRB sample and then check the sample with the Fermi-GBM, Fermi-LAT, and Swift-BAT observations. Based on this sample, the annual detection rate of the SGRB is calculated for HADAR experiments. In the present status, HADAR can detect 0.5 SGRBs in one year. The annual rate can slightly change with different EBL absorption models and intrinsic spec-

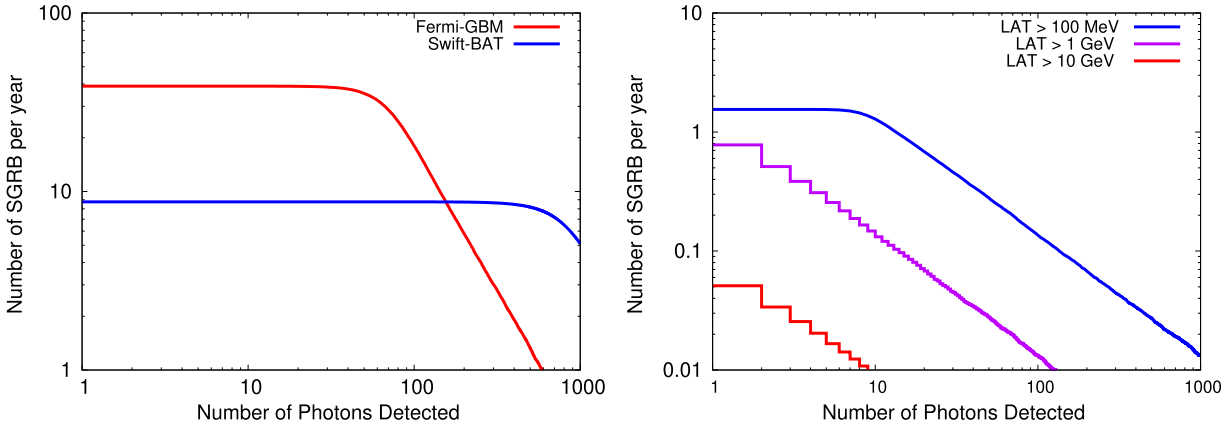

Fig. 4. (color online) Simulated detection rates of SGRBs with the Fermi-GBM, Swift-BAT, and Fermi-LAT. The solid lines represent the cumulative number of detected SGRBs per year as a function of the number of photons detected. The observation rates compared with simulated rates are showed in Table 1.

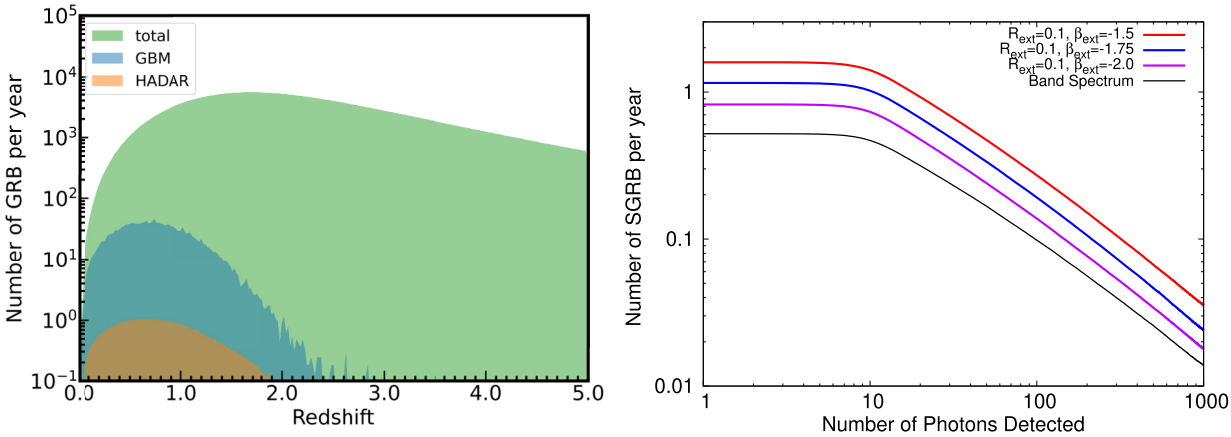

Fig. 5. (color online) Left: SGRB detection rate between the redshifts z and z+dz of the GBM and HADAR, respresented by the blue and orange lines, respectively, whereas the green line denotes the BNS merger rate between the redshifts z and z+dz. Right: SGRB cumulative detection rate of HADAR for different combinations of parameters for the extra component, in which the black line represents the Band spectrum, and the magenta, blue, and red lines represent combinations of the extra + Band components. The model for the EBL absorption described in Ref. [35] is considered, whereas no exponential cutoff is considered.

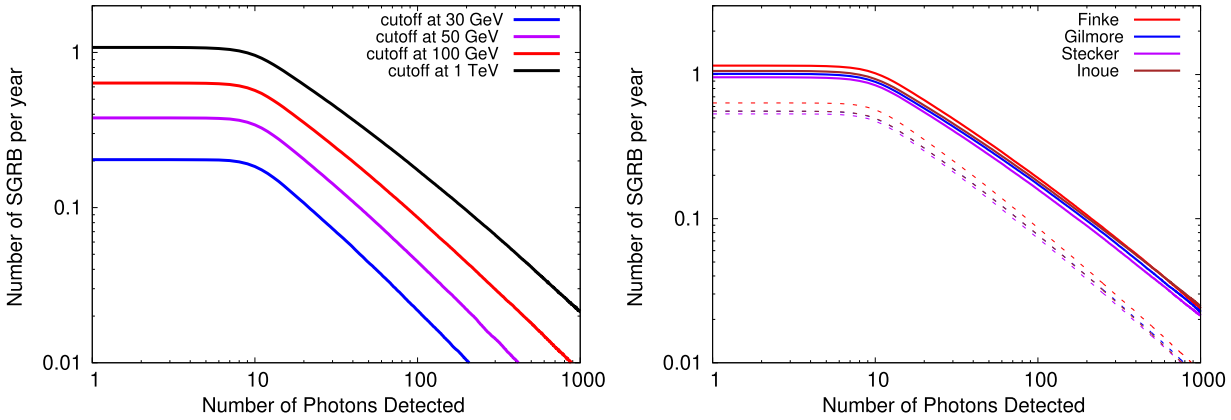

Fig. 6. (color online) Left: SGRB cumulative detection rate with the extra + Band spectra considered for different energy breaks in the case of $\beta_{ext} = -1.75$, $R_{ext} = 0.1$, and the EBL model [35]. Right: SGRB cumulative detection rate with the extra + Band spectra considered for different EBL models, $\beta_{ext} = -1.75$, $R_{ext} = 0.1$. The solid lines are cases without an exponential cutoff, and the dashed lines are the results when the energy spectrum is considered to cut off at 100 GeV.

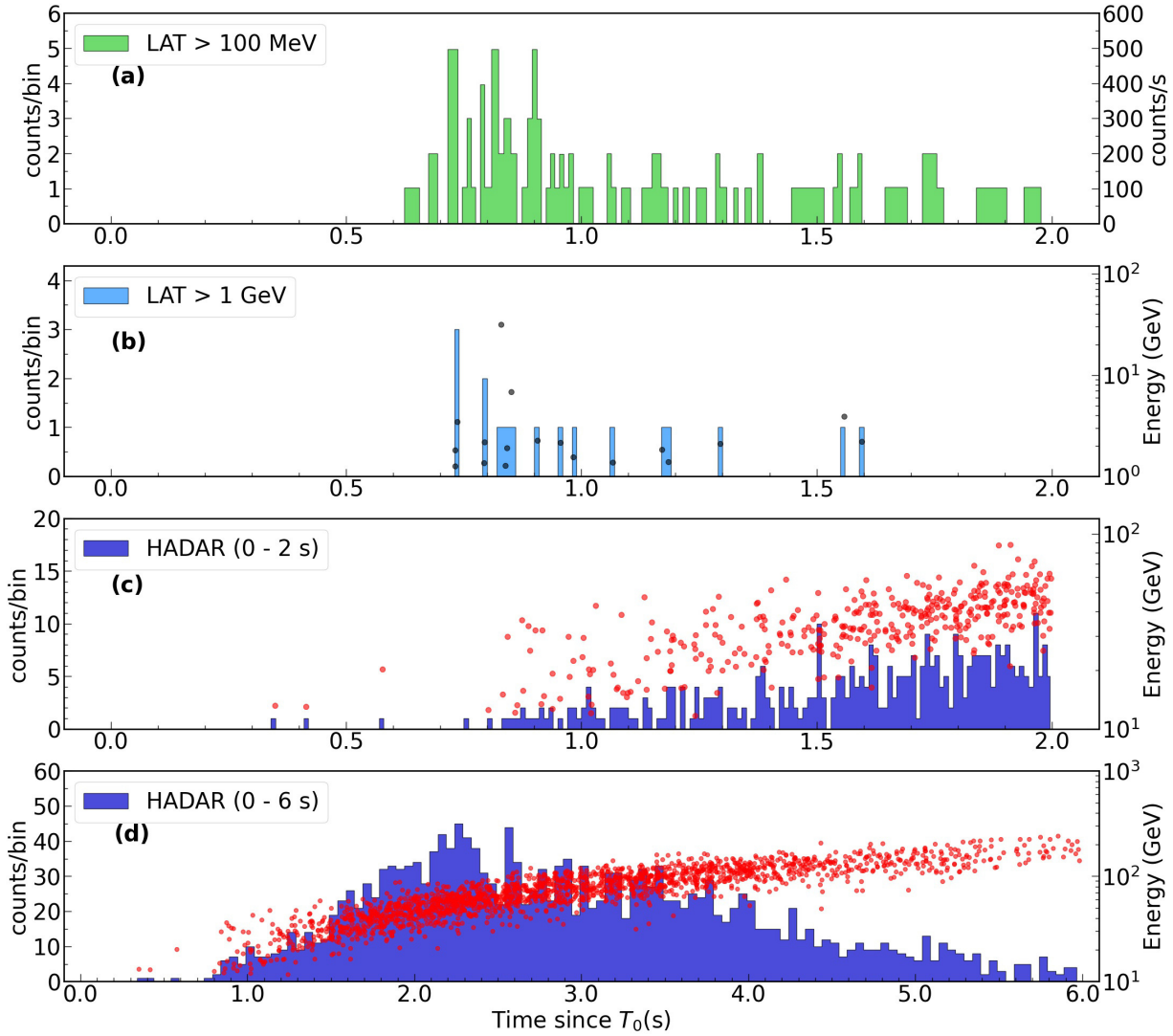

Fig. 7. (color online) Light curves of GRB090510 at different energies. The Fermi-LAT data is taken from Ref. [26]. (a) is for LAT > 100 MeV. The per-second count rate is displayed on the right side for convenience. (b) is for LAT > 1 GeV. (c) A simulated light curve of a 090510-like GRB detected by HADAR. (b), (c), and (d) also overlay the energy versus arrival time for each photon, with the energy scale displayed on the right side. (d) Full light curve described in (c). Photons are represented as gray dots in (b) and red dots in (c) and (d).

tral break-off. Furthermore, we assume that GRB090510A-like events appear in the FOV of HADAR. HADAR can detect approximately 2000 photons with the exponential cutoff considered. HADAR will exhibit good performance in exploring potential new physics, such as LIV. Based on this study, we believe that the HADAR experiment will exhibit good performance in the observation of SGRBs. We hope that the HADAR experiment will be successfully completed and that it will observe SGRBs that are consistent with our expectations in the future.

References

[1] Chryssa Kouveliotou, Charles A. Meegan, Gerald J. Fishman *et al.*, The Astrophysical Journal **413**, L101-L104 (1993)

[2] Peter Meszaros, Reports on Progress in Physics **69**(8), 2259 (2006)

[3] Stan E. Woosley, The Astrophysical Journal **405**, 273-277 (1993)

[4] A. I. MacFadyen and S. E. Woosley, The Astrophysical Journal **524**(1), 262 (1999)

[5] S. I. Blinnikov, I. D. Novikov, T. V. Perevodchikova *et al.*, Soviet Astronomy Letters **10**, 177-179 (1984)

[6] Bohdan Paczynski, The Astrophysical Journal **308**, L43-

L46 (1986)
[7] David Eichler, Mario Livio, Tsvi Piran *et al*., Nature **340**(6229), 126-128 (1989)
[8] Benjamin P. Abbott, Robert Abbott, T. D. Abbott *et al*., The Astrophysical Journal Letters **848**(2), L13 (2017)
[9] D. Band, J. Matteson, L. Ford *et al*., The Astrophysical Journal **413**, 281-292 (1993)
[10] David L. Band, The Astrophysical Journal **588**(2), 945 (2003)
[11] Gor Oganesyan, Lara Nava, Giancarlo Ghirlanda *et al*., The Astrophysical Journal **846**(2), 137 (2017)
[12] Gor Oganesyan, Lara Nava, Giancarlo Ghirlanda *et al*., Astronomy & Astrophysics **616**, A138 (2018)
[13] Gor Oganesyan, Lara Nava, Giancarlo Ghirlanda *et al*., Astronomy & Astrophysics **628**, A59 (2019)
[14] M. E. Ravasio, G. Oganesyan, Giancarlo Ghirlanda *et al*., Astronomy & Astrophysics **613**, A16 (2018)
[15] P. Mészáros and Martin J. Rees, Monthly Notices of the Royal Astronomical Society **269**(1), L41-L43 (1994)
[16] Charles D. Dermer, James Chiang, and Kurt E. Mitman, The Astrophysical Journal **537**(2), 785 (2000)
[17] Re 'em Sari and Ann A. Esin, The Astrophysical Journal **548**(2), 787 (2001)
[18] Bing Zhang and Peter Mészáros, The Astrophysical Journal **559**(1), 110 (2001)
[19] Peter Veres, P. N. Bhat, M. S. Briggs *et al*., Nature **575**(7783), 459-463 (2019)
[20] H. Abdalla, R. Adam, F. Aharonian *et al*., Nature **575**(7783), 464-467 (2019)
[21] H. Abdalla, F. Aharonian *et al*. (H.E.S.S. collaboration), Science **372**(6546), 1081-1085 (2021)
[22] Yong Huang, Shicong Hu, Songzhan Chen *et al*. GRB Coordinates Network, **32677**, 1 (2022)
[23] Giovanni Amelino-Camelia, John Ellis, N. E. Mavromatos *et al*., Nature **393**(6687), 763-765 (1998)
[24] Shota Nakagawa, Fuminobu Takahashi, Masaki Yamada *et al*., Phys. Lett. B **839**, 137824 (2023)
[25] M. M. González, D. Avila Rojas, A. Pratts *et al*., The Astrophysical Journal **944**(2), 178 (2023)
[26] A. A. Abdo, Markus Ackermann, Marco Ajello *et al*., Nature **462**(7271), 331-334 (2009)
[27] J. Bolmont, P. Corona, Philippe Gauron *et al*., Nuclear Instruments and Methods in Physics Research Section A: Accelerators, Spectrometers, Detectors and Associated Equipment **761**, 46-57 (2014)
[28] Jelena Aleksić, S. Ansoldi, Lucio Angelo Antonelli *et al*., Astroparticle Physics **72**, 76-94 (2016)
[29] M. Actis, G. Agnetta *et al*. (CTA Consortium), Experimental Astronomy **32**, 193-316 (2011)
[30] Biswajit Banerjee, Gor Oganesyan, Marica Branchesi *et al*. *Detecting vhe prompt emission from binary neutron-star mergers: Et and cta synergies*, (2022) arXiv: 2212.14007
[31] Guang-Guang Xin, Yu-Hua Yao, Xiang-Li Qian *et al*., The Astrophysical Journal **923**(1), 112 (2021)
[32] LHAASO collaboration , Chinese Physics C **34**(2), 249 (2010)
[33] R. Cornils, S. Gillessen, I. Jung *et al*., Astroparticle Physics **20**(2), 129-143 (2003)
[34] M. Wood, T. Jogler, Jonathan Dumm, and S. Funk, Astroparticle Physics **72**, 11-31 (2016)
[35] Justin D. Finke, Soebur Razzaque, and Charles D. Dermer, The Astrophysical Journal **712**(1), 238 (2010)
[36] Bing Zhang. *The physics of gamma-ray bursts*, (Cambridge University Press, 2018)
[37] PDG Particle Data Group. Particle Physics Booklet, 2020
[38] E. J. Howell, K. Ackley, A. Rowlinson *et al*., Monthly Notices of the Royal Astronomical Society **485**(1), 1435-1447 (2019)
[39] Tania Regimbau and Scott A. Hughes, Physical Review D **79**(6), 062002 (2009)
[40] Piero Madau and Mark Dickinson, Annual Review of Astronomy and Astrophysics **52**, 415-486 (2014)
[41] David Wanderman and Tsvi Piran, Monthly Notices of the Royal Astronomical Society **448**(4), 3026-3037 (2015)
[42] Jun Kakuwa, Kohta Murase, Kenji Toma *et al*., Monthly Notices of the Royal Astronomical Society **425**(1), 514-526 (2012)
[43] S. Poolakkil, R. Preece, C. Fletcher *et al*., The Astrophysical Journal **913**(1), 60 (2021)
[44] Ryo Tsutsui, Daisuke Yonetoku, Takashi Nakamura *et al*., Monthly Notices of the Royal Astronomical Society **431**(2), 1398-1404 (2013)
[45] Markus Ackermann, K. Asano, W. B. Atwood *et al*., The Astrophysical Journal **716**(2), 1178 (2010)
[46] Markus Ackermann, Marco Ajello, K. Asano *et al*., The Astrophysical Journal **729**(2), 114 (2011)
[47] Katsuaki Asano and Susumu Inoue, The Astrophysical Journal **671**(1), 645 (2007)
[48] Ye Chen, Ruo-Yu Liu, and Xiang-Yu Wang, Monthly Notices of the Royal Astronomical Society **478**(1), 749-757 (2018)
[49] Jagdish C. Joshi and Soebur Razzaque, Monthly Notices of the Royal Astronomical Society **505**(2), 1718-1729 (2021)
[50] G. Ghisellini, G. Ghirlanda, L. Nava *et al*., Monthly Notices of the Royal Astronomical Society **403**(2), 926-937 (2010)
[51] A. Von Kienlin, C. A. Meegan, W. S. Paciesas *et al*., The Astrophysical Journal **893**(1), 46 (2020)
[52] Amy Lien, Takanori Sakamoto, Scott D. Barthelmy *et al*., The Astrophysical Journal **829**(1), 7 (2016)
[53] M. Ajello, M. Arimoto, Magnus Axelsson *et al*., The Astrophysical Journal **878**(1), 52 (2019)
[54] Rudy C. Gilmore, Rachel S. Somerville, Joel R. Primack *et al*., Monthly Notices of the Royal Astronomical Society **422**(4), 3189-3207 (2012)
[55] Floyd W. Stecker, Matthew A. Malkan, and Sean T. Scully, The Astrophysical Journal **761**(2), 128 (2012)
[56] Yoshiyuki Inoue, Susumu Inoue, Masakazu A.R. Kobayashi *et al*., The Astrophysical Journal **768**(2), 197 (2013)